

Precision Dose-Finding Design for Phase I Oncology Trials by Integrating Pharmacology Data

Kyong Ju Lee¹ and Yuan Ji²

¹Department of Statistics, The University of Chicago

²Department of Public Health Sciences, The University of Chicago

January 13, 2026

Abstract

Phase I oncology trials aim to identify a safe dose—often the maximum tolerated dose (MTD)—for subsequent studies. Conventional designs focus on population-level toxicity modeling, with recent attention on leveraging pharmacokinetic (PK) data to improve dose selection. We propose the Precision Dose-Finding (PDF) design, a novel Bayesian phase I framework that integrates individual patient PK profiles into the dose-finding process. By incorporating patient-specific PK parameters (such as volume of distribution V_i and elimination rate k_i), PDF models toxicity risk at the individual level, in contrast to traditional methods that ignore inter-patient variability. The trial is structured in two stages: an initial training stage to update model parameters using cohort-based dose escalation, and a subsequent test stage in which doses for new patients are chosen based on each patient's own PK-predicted toxicity probability. This two-stage approach enables truly personalized dose assignment while maintaining rigorous safety oversight. Extensive simulation studies demonstrate the feasibility of PDF and suggest that it provides improved safety and dosing precision relative to the continual

reassessment method (CRM). The PDF design thus offers a refined dose-finding strategy that tailors the MTD to individual patients, aligning phase I trials with the ideals of precision medicine.

Keywords: Bayesian design; Dose response; Pharmacodynamics; Pharmacokinetics; Toxicity.

1 Introduction

Phase I oncology trials are designed to evaluate drug safety and determine an appropriate dose for further testing, like the maximum tolerated dose (MTD) defined as the highest dose with a toxicity rate not higher than a target rate. Dose-finding designs have traditionally fallen into two broad categories: simple algorithmic rule-based designs (such as the 3+3 and i3+3) and model-based designs that utilize statistical modeling of dose-toxicity relationships (Storer, 1989; Liu et al., 2020; O’Quigley et al., 1990; Ji et al., 2010; Guo et al., 2017; Liu and Yuan, 2015). Most designs assume that all patients share the same dose-toxicity relationship, ignoring individual heterogeneity in drug response.

In recognition of the limitations of the one-size-fits-all paradigm, efforts to incorporate patient-specific data—particularly pharmacokinetic (PK) measurements—into dose-finding began decades ago. For example, Piantadosi and Liu (1996) pioneered integrating PK information into a dose-toxicity model. Subsequent methods introduced summary PK exposure metrics, such as the area under the concentration-time curve (AUC) or maximum concentration (C_{\max}), as covariates in logistic or probit models for toxicity outcomes (Whitehead et al., 2007; Ursino et al., 2017). These approaches demonstrated that using PK data can better capture the dose-toxicity relationships, even in small trials. In particular, Toumazi et al. (2018) showed that incorporating PK measurements during dose escalation improved the estimation of the dose-toxicity curve without compromising the accuracy of MTD identification. More recently, semi-mechanistic designs have modeled the entire PK/PD time-course for each patient. Notably, the SDF design (Su et al., 2022) and the extended Bayesian semi-mechanistic design of Yang and Li (2024) used longitudinal PK and latent pharmacodynamic (PD) data to update toxicity probabilities,

maintaining robust inference despite limited sample sizes. Building on their work, the PEDOOP design (Yuan et al., 2024) separated the roles of PK and PD predictors for toxicity and efficacy, respectively, further bridging pharmacology and dose-finding. Each of these innovations represents a step toward more individualized dosing.

Despite these advances, most current phase I designs continue to base dose decisions on population averages rather than individual patient characteristics. This can be problematic because patients vary widely in factors like organ function, comorbidities, and metabolism, which influence their ability to tolerate drugs (Nikanjam et al., 2023). The authors also note that traditional flat dosing fails to account for such variability, making it challenging to determine “the right dose for each patient”. Recent research has underscored the benefits of accounting for patient heterogeneity. For instance, Ollier and Mozgunov (2025) demonstrated that failing to include important patient covariates in a dose-finding model can drastically reduce the chance of selecting the correct dose and increase the risk of overdosing. Likewise, Silva et al. (2024) proposed a precision dose-escalation design that identifies subgroups of patients with different MTDs when eligibility criteria are broadened. In their approach, patients are stratified into subpopulations *a priori* or via sequential modeling, and separate MTDs are estimated for each subgroup. Such subpopulation-based designs represent progress toward personalized dosing, but they stop short of true N-of-1 dose adaptation since patients within each subgroup still receive the same recommended dose. Early work by Babb and Rogatko (2001) took the next step by deriving an individual MTD as a monotonic function of each patient’s baseline anti-SEA antibody concentration, using the EWOC framework to control overdose probability. However, their method does not incorporate PK parameters.

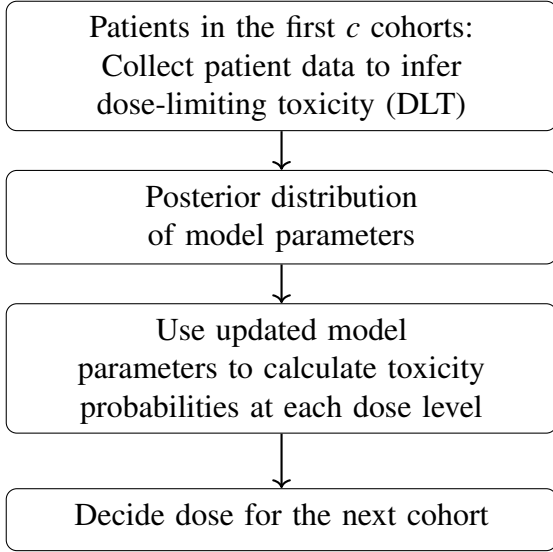
In this work, we introduce the Precision Dose-Finding (PDF) design, which achieves fully individualized dose selection by integrating each patient’s own PK profile into the dose assignment process. The PDF design extends the PEDOOP framework one step further: rather than linking individual PK data to a population-level AUC metric, it uses each patient’s personal PK parameters directly in the model. Specif-

ically, we assume a one-compartment PK model for each patient with individual volume of distribution (V_i) and elimination rate (k_i), allowing us to compute that patient's drug exposure (AUC) and predict their toxicity risk in real time. By modeling toxicity probability as a function of patient-specific PK characteristics, the PDF method aligns with the paradigm of precision medicine and directly addresses the challenge of inter-patient variability in tolerance.

PDF comprises a training stage and a test stage (Figure 1.1). During the training stage, patients are treated in cohorts using a conventional model-based escalation procedure to safely explore the dose range and iteratively update model parameters with accumulating toxicity and PK data. Once sufficient information has been gathered, the trial transitions to the test stage. In this stage, dose assignment becomes fully personalized: baseline characteristics of each new patient will be measured, and their PK parameters predicted. Based on the predicted PK parameters, a predicted toxicity probability at each dose will be computed using the training data. The predicted MTD for that patient will then be administered to the patient. The model is continually updated with each treated patient, and learning continues in the test stage. This two-stage design ensures that the personalized dosing strategy is grounded in prior data and that its performance is validated in real time, thereby safeguarding patient safety while maximizing the precision of dose recommendations.

We will begin with introducing the model assumptions of PDF in Section 2.1, and explain how to allocate patients during the “training” stage in Section 2.2. Next, Section 2.3 will describe how the MTD of a trial can be determined, and Section 2.4 will describe how to perform precision dose-finding. In Section 3, we will present the simulation results and compare them with the popular CRM design to evaluate the viability and performance of our approach. In Section 4, we end the article with a brief discussion.

Training Stage (Stage I)



Test Stage (Stage II)

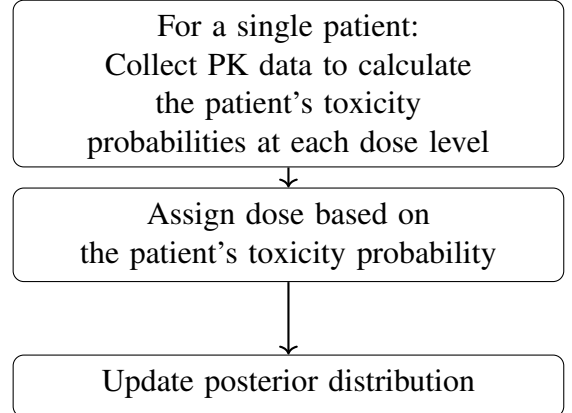


Figure 1.1: Schema of the PDF design. The training stage allocates patients using a conventional dose escalation method and focuses on updating model parameters. The test stage assigns doses to individual patients based on their personal toxicity probabilities derived from PK data.

2 Methods

2.1 Probability Model

For PK modeling, we assume a one-compartmental model for simplicity, which treats the human body as a single, uniform compartment and administers drugs via intravenous (IV) injection. Furthermore, we assume a first-order process to describe the rate of drug absorption and elimination (Shargel et al., 1999).

Let $c_i(t)$ denote the drug concentration of patient $i \in \{1, \dots, N\}$ at time t after drug administration. The rate of a first-order process is $dc_i(t)/dt = -k_i c_i(t)$, with initial concentration $c_i(0) = d_i/V_i$. This yields the drug plasma concentration for patient i at time t as

$$c_i(t|d_i, V_i, k_i) = \frac{d_i}{V_i} e^{-k_i t} \quad (1)$$

where d_i is one of the D drug dosages administered to patient i , $d_i \in \{1, \dots, D\}$, k_i denotes the patient-specific elimination rate constant, and V_i is the patient-specific volume of distribution. We also assume $V_i > 0$ and $k_i > 0$ follow some prior distributions (e.g., gamma or log-normal) with hyperparameters α

and λ . In our earlier work PEDOOP (Yuan et al., 2024), the priors for V_i and k_i can only take gamma distributions, a restriction we relax here.

Let X_{ij} denote the observed drug concentration at time $t_j \in \{1, \dots, T\}$ for patient i . We assume X_{ij} follows a log normal distribution:

$$\log(X_{ij}) = \log(c_i(t_j | d_i, V_i, k_i)) + \varepsilon_{ij}, \text{ and } \varepsilon_{ij} \sim N(0, \sigma^2) \quad (2)$$

where ε_{ij} represents random error.

As described in PEDOOP, we compute the area under the concentration-time curve (AUC) for patient i by integrating the drug concentration $c_i(t | d_i, V_i, k_i)$ from 0 to ∞ :

$$AUC_i(d_i, V_i, k_i) = \int_0^\infty c_i(t | d_i, V_i, k_i) dt = \frac{d_i}{V_i k_i}. \quad (3)$$

Next, we incorporate the AUC of patient i as a covariate in modeling their toxicity probability. Specifically, let p_i denote the toxicity probability for patient i and assume

$$\begin{aligned} p_i &\triangleq p_i(V_i, k_i, \beta_0, \beta_1) = \text{logit}^{-1}(\beta_0 + \beta_1 \times \log AUC_i(d_i, V_i, k_i)) \\ &= \text{logit}^{-1}(\beta_0 + \beta_1 \times \log \frac{d_i}{V_i k_i}), \end{aligned} \quad (4)$$

where $\text{logit}^{-1}(x) = 1/(1 + e^{-x})$.

Let Y_i denote the binary DLT outcome for patient i and Y_i follows a Bernoulli distribution given by

$$Y_i | V_i, k_i, \beta_0, \beta_1 \sim \text{Bernoulli}(p_i(V_i, k_i, \beta_0, \beta_1)). \quad (5)$$

As a result, the joint posterior distribution of all parameters $\boldsymbol{\theta} = (V_i, k_i, \alpha_V, \lambda_V, \alpha_k, \lambda_k, \beta_0, \beta_1, \sigma^2)$ given

the observed data $\mathcal{D}_I = \{(X_{ij}, Y_i, d_i)\}$, becomes

$$\begin{aligned}
\pi(\boldsymbol{\theta} | \mathcal{D}_I) \propto & \prod_i^N \prod_j^T \frac{1}{\sigma \sqrt{2\pi}} \exp \left(-\frac{(\log(X_{ij}) - \log(c_i(t_j | d_i, V_i, k_i)))^2}{2\sigma^2} \right) \\
& \times \prod_i^N p_i^{Y_i} (1 - p_i)^{1 - Y_i} \\
& \times \prod_i^N g(V_i | \alpha_V, \lambda_V) \times g(k_i | \alpha_k, \lambda_k) \\
& \times h(\beta_0) \times h(\beta_1) \\
& \times h(\alpha_V) \times h(\lambda_V) \times h(\alpha_k) \times h(\lambda_k) \times h(\sigma^2).
\end{aligned}$$

Here, $g(\cdot)$ and $h(\cdot)$ denotes the corresponding prior distribution functions. We adopt the hyper-prior distributions from PEDOOP, given by

$$\begin{aligned}
\alpha_V & \sim \text{Gamma}(4, 1), \lambda_V \sim \text{Gamma}(1, 1) \\
\alpha_k & \sim \text{Gamma}(3, 1), \lambda_k \sim \text{Gamma}(1, 1) \\
\sigma & \sim \text{Gamma}(3, 3), \beta_0 \sim N(-3, 100), \beta_1 \sim \log N(-1, 2).
\end{aligned} \tag{6}$$

These priors have been shown to lead to weak information on the p_i 's (Yuan et al., 2024). Using the Markov chain Monte Carlo (MCMC) algorithm, we can generate posterior samples of $\boldsymbol{\theta} = (V_i, k_i, \alpha_V, \lambda_V, \alpha_k, \lambda_k, \beta_0, \beta_1, \sigma^2)$.

2.2 Stage I: Cohort-Based Dose Escalation

For the first c cohorts, each with a fixed number of patients, we follow the conventional dose allocation rules, that is, assigning the same dose level to patients within the same cohort. Starting from the lowest dose level, we use the dose-level toxicity probability \tilde{p}_d (defined next) to determine the appropriate dose for the next cohort via posterior predictive inference.

Assume n patients have been enrolled in the trial so far. Let \mathcal{D}_I represent the cumulative data of stage

I. Let Y_{new} denote the DLT outcome of a new patient in the next cohort treated at the dose level $Z_{new} = d$.

The predictive toxicity probability \tilde{p}_d is computed as

$$\begin{aligned}
\tilde{p}_d &\triangleq \Pr(Y_{new} = 1 | \mathcal{D}_I, Z_{new} = d) \\
&= \int \Pr(Y_{new} = 1 | V_{new}, k_{new}, \beta_0, \beta_1, Z_{new} = d) \pi(V_{new}, k_{new}, \beta_0, \beta_1 | \mathcal{D}_I) dV_{new} dk_{new} d\beta_0 d\beta_1 \\
&= \int \text{logit}^{-1}(\beta_0 + \beta_1 \times \log \frac{d}{V_{new} k_{new}}) \pi(V_{new}, k_{new}, \beta_0, \beta_1 | \mathcal{D}_I) dV_{new} dk_{new} d\beta_0 d\beta_1 \\
&\approx \frac{1}{M} \sum_{m=1}^M \text{logit}^{-1}(\beta_0^{(m)} + \beta_1^{(m)} \log \frac{d}{V_{new}^{(m)} k_{new}^{(m)}}),
\end{aligned} \tag{7}$$

where notation (m) denotes the m th sample from the MCMC simulation for the joint posterior $\pi(\boldsymbol{\theta} | \mathcal{D}_I)$, and $V_{new}^{(m)} = \sum_{i=1}^n \frac{V_i^{(m)}}{n}$ and $k_{new}^{(m)} = \sum_{i=1}^n \frac{k_i^{(m)}}{n}$ for the new patients in the next cohort. When the trial just starts, \mathcal{D}_I is an empty set and $\pi(V_{new}, k_{new}, \beta_0, \beta_1 | \mathcal{D}_I)$ becomes the prior distribution of V_{new} and k_{new} .

Following the CRM (O’Quigley et al., 1990), we choose the dose \tilde{d} for the next cohort where

$$\tilde{d} = \arg \min_d |\tilde{p}_d - p_T| \tag{8}$$

and p_T is a prespecified target toxicity rate (e.g., 0.3).

In addition, we apply the following rules to enhance the efficiency and safety of the trial.

- **Speed-up rule:** If no DLT outcomes are observed in any tested dose levels, escalate to the next higher dose for the next cohort to accelerate exploration.
- **Safety rule 1 (no skip):** If Equation (8) suggests that the dose should increase by two or more levels, we restrict escalation to only one level for the next cohort to address safety concerns (Goodman et al., 1995).
- **Safety rule 2 (dose exclusion & early termination, Ji et al. (2007)):** Let n_d denote the number of patients treated at dose level d , and let Y_d represent the number of patients who experienced

DLT at dose level d . Assume the prior distribution for the toxicity probability at dose d is $p_d \sim Beta(0.05, 0.05)$, and the DLT outcome follows $Y_d | p_d \sim Bin(n_d, p_d)$. The posterior distribution of toxicity probability at dose d is then $p_d | Y_d \sim Beta(Y_d + 0.05, n_d - Y_d + 0.05)$. A dose is regarded as safe if it satisfies

$$Pr(p_d > p_T | Y_d, n_d) < s^* \quad (9)$$

where p_T is the prespecified target toxicity rate and s^* is a preselected safety threshold. If the suggested dose \tilde{d} from (8) is not safe, the algorithm instead recommends the highest dose that meets (9) for the next cohort. If no dose meets this criterion, the trial will be terminated. Otherwise, the algorithm recommends the highest dose that satisfies both (8) and (9) for the next cohort.

- **Coherence principle:** At the end of the decision-making process, one more constraint is added to ensure escalation coherence (Cheung, 2005). Suppose the current dose is d , and the recommended next dose based on the dose escalation rules described above is d^* . If the proportion of DLT outcomes at the current dose, i.e., Y_d / n_d , exceeds the target p_T and $d^* > d$, do not escalate; instead, stay at the current dose for the next cohort. Conversely, if $Y_d / n_d < p_T$ and $d^* < d$, do not de-escalate, and instead, stay at the current dose level for the next cohort.

2.3 MTD Selection for Stage I

Once all patients in the first c cohorts have been treated, we can select the MTD for the training stage. To determine the MTD, we suggest comparing the posterior summary statistic of the dose-level toxicity probability \hat{p}_d with the target toxicity probability p_T , and selecting the dose that minimizes the difference. As described in Safety rule 2, assuming a beta prior and a binomial distribution for DLT outcomes, the

posterior mean of the toxicity probability at dose d is:

$$\hat{p}_d = \frac{Y_d + 0.05}{n_d + 0.1}$$

Note that, to determine the MTD, \hat{p}_d is transformed via isotonic regression to \hat{p}_d^* using the pool adjacent violators algorithm (Robertson et al., 1988), which guarantees the monotonicity of the dose-toxicity relationship.

Consequently, we select the dose as the MTD for stage I that satisfies

$$d^{MTD} = \arg \min_d |\hat{p}_d^* - p_T| \quad (10)$$

from among the tested doses that are deemed safe using criterion (9). Since \hat{p}_d^* can be tied, we choose the MTD by the following rule:

- (1) If $\hat{p}_{d^{MTD}} > p_T$, the MTD is the lowest dose among tied doses.
- (2) If $\hat{p}_{d^{MTD}} \leq p_T$, the MTD is the highest dose among tied doses.

2.4 Stage II: Precision Dose-Finding

In precision dose-finding, each patient receives a predicted MTD using the posterior information learned from stage I. We recommend that 30% of the total number of patients be treated under the precision dose-finding scheme, or that the training sample size be set to at least 21, which is typical for phase I trials. Instead of following the dose escalation rules introduced in Section 2.2 to determine dosage, we administer the dose based on each patient's individual toxicity profile.

Specifically, for each patient, we estimate the predicted toxicity probability of patient i if s/he is

treated at dose d by

$$\hat{p}_{i,d} = \text{logit}^{-1}(\hat{\beta}_0 + \hat{\beta}_1 \times \log \frac{d}{\hat{V}_i \hat{k}_i}), \quad (11)$$

where $\hat{\beta}_0$ and $\hat{\beta}_1$ are the posterior means of β_0 and β_1 from the first stage dose-finding, respectively. (\hat{V}_i, \hat{k}_i) represent pre-dose predicted PK parameters for patient i . In precision dose-finding, we assume that individual PK parameters can be either directly measured or reliably predicted. In practice, one can obtain (\hat{V}_i, \hat{k}_i) from a population PK (popPK) nonlinear mixed-effects model fit to Stage I PK data, combined with baseline covariates (e.g., body size and renal/hepatic function). Further details are provided in Section 4.

In addition, the model parameters will continue to be updated as new data becomes available. Then patient i is assigned to dose d_i^* given by

$$d_i^* = \arg \min_d |\hat{p}_{i,d} - p_T|. \quad (12)$$

As a result, each new patient receives the dose that satisfies both (12) and (9). This continues until the maximum number of patients for the trial is reached. Note that, as this precision dose-finding approach is implemented, selecting a single MTD for the overall trial becomes optional, since each patient is associated with their own MTD d_i^* .

3 Simulation Study

3.1 Simulation Setup

We conducted simulation studies of the PDF design under different scenarios and compared the results with the CRM design. Following the guidance of Goodman et al. (1995), we performed 1,000 trials

across five distinct scenarios. Each scenario varied the true coefficient parameters β_0 and β_1 , under the assumption that one of the dose levels is the true MTD. The true coefficient pairs used in these scenarios were $\{(-3, 1.5), (-4, 1.5), (-4.5, 1.5), (-2.5, 0.6), (-1, 1.2)\}$.

For $\boldsymbol{\theta} = (V_i, k_i, \alpha_V, \lambda_V, \alpha_k, \lambda_k, \beta_0, \beta_1, \sigma^2)$, we assume the prior distributions described in (6). In this simulation, V_i and k_i were assumed to follow gamma distributions, i.e., $V_i \sim \text{Gamma}(4, 1)$, $k_i \sim \text{Gamma}(3, 1)$, which is the same as PEDOOP. However, later in Section 3.3.1 we also conducted a sensitivity analysis using different prior distributions.

The target toxicity rate was set to $p_T = 0.3$. Simulated trials assumed five discrete dose levels $d \in \{15, 30, 60, 90, 120\}$ and measured the drug concentration of each patient at time points $t_j \in \{1, 3, 5, 7, 12, 24\}$ hours after injection. A total of 30 patients was enrolled for each trial, with the first 21 receiving doses using the traditional dose-finding algorithm for stage I, and the remaining 9 patients following the precision dose-finding approach for stage II. We set $s^* = 0.95$ in (9).

Note that due to the structure of our model, the true toxicity probability at each dose level did not exist. Instead, we generated 2,000 random pairs of V_i and k_i from their prior distributions and plugged them into (4), along with true β_0 and β_1 , to simulate the true average toxicity probability for each dose level, averaged across the 2,000 simulated patients. These simulated averages were reported as “True avg p_d ” in the first line of each scenario in Tables 3.1 and 3.2.

The CRM design was based on the model $p_d = \phi_d^{\exp(-\beta)}$, $d = 1, \dots, 5$, where the skeleton $\phi = (\phi_1, \dots, \phi_5)$ was a set of prior guesses on toxicity probabilities at each dose level, and β followed a normal prior distribution with mean 0 and standard deviation 2. For fair comparison, the CRM design sample size was set to 21.

3.2 Simulation Results

The simulation results of our approach are presented in Tables 3.1 and 3.2, reporting the results of the first 21 patients and the last 9 patients, respectively. “SC” denotes scenarios from 1 to 5; “True avg p_d ”

represents the true average toxicity rates at each dose level; “ Y_d/n_d ” is the empirical toxicity rate at dose d ; “ n_d ” is the average number of patients assigned to each dose level over 1,000 simulated trials; finally, “Sel%” is the proportion of simulated trials in which each dose is selected as the MTD. “No MTD” indicates early termination or failure to recommend a safe MTD.

In scenarios 1 and 2, the true MTDs are dose levels 2 and 3, respectively. The proposed PDF design demonstrates strong performance in both scenarios, achieving the highest Sel% at the correct doses. Moreover, the highest n_d values also occur at the correct MTDs, showing efficient patient allocation. In addition, PDF allocates fewer patients and selects MTDs less frequently at overly toxic dose levels.

Both PDF and CRM designs assign the most patients to dose level 3 in scenario 3, where the true MTD is dose level 4. However, the PDF design assigns a slightly higher average number of patients (n_d) to this dose level compared to the CRM. Additionally, both the PDF design and the CRM correctly identify the true MTD. Notably, our approach assigns fewer patients to, and selects less frequently, the overly toxic dose level 5 compared to CRM.

Scenario 4 presents a challenging case in which dose levels 3 – 5 are all close to the target p_T . PDF and CRM perform comparably, allocating patients to mostly dose levels 3 and 4. With larger sample sizes, both designs may eventually recognize dose level 5 as the true MTD. In scenario 5, all doses are overly toxic. PDF assigns slightly fewer patients to toxic doses with much lower incorrect MTD selection.

Table 3.2 presents the simulation results for the last nine patients, who underwent precision dose-finding. Row 2 of each scenario presents Y_d^*/n_d^* , where n_d^* and Y_d^* are the numbers of patients among the last nine that are assigned to dose level d and that experience DLT at dose level d , respectively. We can see that most Y_d^*/n_d^* values are around or smaller than $p_T = 0.3$, regardless of the true average p_d values. This shows the benefit of precision dose-finding, since each patient is assigned based on his/her PK-implied optimal dose, regardless of what the expected toxicity rate p_d is.

In the test stage, each patient’s dose is determined by his or her own PK profile. Because these PK

Table 3.1: Simulation results of the first 21 patients of scenarios 1 to 5. The column having a bold-faced number is the true MTD of that scenario.

Dose levels		1	2	3	4	5	No MTD
SC 1	True avg p_d	0.151	0.287	0.470	0.586	0.665	–
	PDF Y_d/n_d	0.153	0.290	0.473	0.600	0.583	–
	n_d	6.255	8.808	5.028	0.717	0.024	–
	Sel%	0.160	0.540	0.257	0.032	0.001	0.010
	CRM n_d	7.698	7.821	4.677	0.756	0.048	–
	Sel%	0.158	0.503	0.299	0.038	0.002	0.000
SC 2	True avg p_d	0.073	0.156	0.293	0.397	0.478	–
	PDF Y_d/n_d	0.066	0.154	0.300	0.400	0.458	–
	n_d	3.891	5.805	7.203	3.459	0.627	–
	Sel%	0.014	0.193	0.435	0.286	0.071	0.001
	CRM n_d	4.176	5.778	6.903	3.354	0.789	–
	Sel%	0.006	0.131	0.426	0.329	0.108	0.000
SC 3	True avg p_d	0.049	0.110	0.220	0.310	0.385	–
	PDF Y_d/n_d	0.044	0.109	0.220	0.319	0.361	–
	n_d	3.516	4.659	6.447	4.746	1.632	–
	Sel%	0.004	0.055	0.298	0.399	0.228	0.016
	CRM n_d	3.642	4.617	6.345	4.455	1.941	–
	Sel%	0.000	0.040	0.248	0.405	0.307	0.000
SC 4	True avg p_d	0.111	0.158	0.218	0.260	0.293	–
	PDF Y_d/n_d	0.112	0.162	0.218	0.277	0.279	–
	n_d	4.671	5.445	5.472	3.819	1.539	–
	Sel%	0.019	0.114	0.291	0.324	0.249	0.003
	CRM n_d	4.896	5.361	5.634	3.432	1.677	–
	Sel%	0.012	0.107	0.262	0.315	0.304	0.000
SC 5	True avg p_d	0.422	0.593	0.747	0.819	0.860	–
	PDF Y_d/n_d	0.427	0.602	0.716	0	0	–
	n_d	13.146	2.643	0.162	0	0	–
	Sel%	0.494	0.031	0.002	0	0	0.473
	CRM n_d	19.131	1.713	0.156	0	0	–
	Sel%	0.952	0.047	0.001	0	0	0.000

values are predictions rather than directly observed quantities, they are subject to estimation error. To

Table 3.2: Simulation results of the last nine patients of scenarios 1 to 5. The column having a bold-faced number is the true MTD of that scenario.

Dose levels		1	2	3	4	5
SC 1	True avg p_d	0.151	0.287	0.470	0.586	0.665
	Y_d^*/n_d^*	0.322	0.190	0.256	0.272	0.215
	n_d^*	2.668	3.297	1.458	0.581	0.901
SC 2	True avg p_d	0.073	0.156	0.293	0.397	0.478
	Y_d^*/n_d^*	0.332	0.216	0.232	0.244	0.174
	n_d^*	0.834	1.836	1.999	1.302	3.020
SC 3	True avg p_d	0.049	0.110	0.220	0.310	0.385
	Y_d^*/n_d^*	0.426	0.250	0.247	0.242	0.142
	n_d^*	0.646	1.062	1.548	1.266	4.478
SC 4	True avg p_d	0.111	0.158	0.218	0.260	0.293
	Y_d^*/n_d^*	0.341	0.248	0.261	0.240	0.151
	n_d^*	0.615	0.940	1.103	1.048	5.260
SC 5	True avg p_d	0.422	0.593	0.747	0.819	0.860
	Y_d^*/n_d^*	0.381	0.279	0.263	0.323	0.154
	n_d^*	3.718	0.502	0.133	0.031	0.026

model this, we consider adding errors to V_i and k_i and assume

$$\hat{V}_i = V_i + e_i, \quad e_i \sim \text{Truncated Normal}(0, \frac{\sigma_V^2}{9}, -V_i, \infty)$$

$$\hat{k}_i = k_i + g_i, \quad g_i \sim \text{Truncated Normal}(0, \frac{\sigma_k^2}{9}, -k_i, \infty)$$

where each error term has mean 0, variance equal to 1/9 of the true variance, and is truncated below at the negative of its true value to prevent negative PK parameters. When dosing, we compute $\hat{p}_{i,d}$ by substituting \hat{V}_i and \hat{k}_i into the model. Table 3.3 summarizes the simulation results under this framework. Although toxicity rates increased slightly, the overall pattern remains unchanged, demonstrating that the precision dose-finding stage is robust to realistic PK-prediction errors.

Figure 3.1 displays the dose chosen for the last patient (# 30) in each scenario. In general, the largest bubble (count) increases in SC 1 to 4, whereas SC5 keeps the patient at the lowest dose level. The DLT

Table 3.3: Simulation results of the last nine patients of scenarios 1 to 5 (with prediction errors of V_i and k_i)

Dose levels		1	2	3	4	5
SC 1	True avg p_d	0.151	0.287	0.470	0.586	0.665
	Y_d^*/n_d^*	0.375	0.204	0.246	0.286	0.213
	n_d^*	2.879	3.133	1.425	0.574	0.890
SC 2	True avg p_d	0.073	0.156	0.293	0.397	0.478
	Y_d^*/n_d^*	0.408	0.226	0.219	0.249	0.181
	n_d^*	1.076	1.742	1.947	1.271	2.953
SC 3	True avg p_d	0.049	0.110	0.220	0.310	0.385
	Y_d^*/n_d^*	0.426	0.250	0.247	0.242	0.142
	n_d^*	0.646	1.062	1.548	1.266	4.478
SC 4	True avg p_d	0.111	0.158	0.218	0.260	0.293
	Y_d^*/n_d^*	0.387	0.271	0.271	0.234	0.162
	n_d^*	0.764	0.971	1.049	1.165	5.018
SC 5	True avg p_d	0.422	0.593	0.747	0.819	0.860
	Y_d^*/n_d^*	0.408	0.238	0.362	0.167	0.259
	n_d^*	3.700	0.525	0.116	0.030	0.027

rates in each scenario are all below $p_T = 0.3$, implying that the precision-based dosing is safe.

We also present outcomes of six randomly selected trials from scenario 1 (Figure 3.2). It displays dose escalation patterns for the first 21 patients and varying dose assignments for the last 9 patients, who participated in the precision dose-finding. Notably, the last 9 patients tend to receive doses centered near the true MTD. The plots further reveal that some patients received the same dose but experienced different DLT outcomes. For instance, patient 22, 23, and 30 in “SC1 - Trial3” had PK profiles (V_i, k_i) of $(6.53, 3.18)$, $(1.80, 1.65)$, and $(1.51, 1.34)$. Other trials, not shown here, also suggest that patients with a higher V_i/k_i ratio may be more likely to experience DLT.

To further illustrate the precision dose-finding, in Figure 3.3 we report the predicted MTD for a patient with different values of V_i and k_i , given by $d_i = V_i k_i \exp\left(\frac{\logit(p_i) - \hat{\beta}_0}{\hat{\beta}_1}\right)$, rounded up to the nearest tested dose, where $p_i = 0.3$ and the coefficients are set to their posterior means. It can be seen that as

Dose Chosen for Patient #30

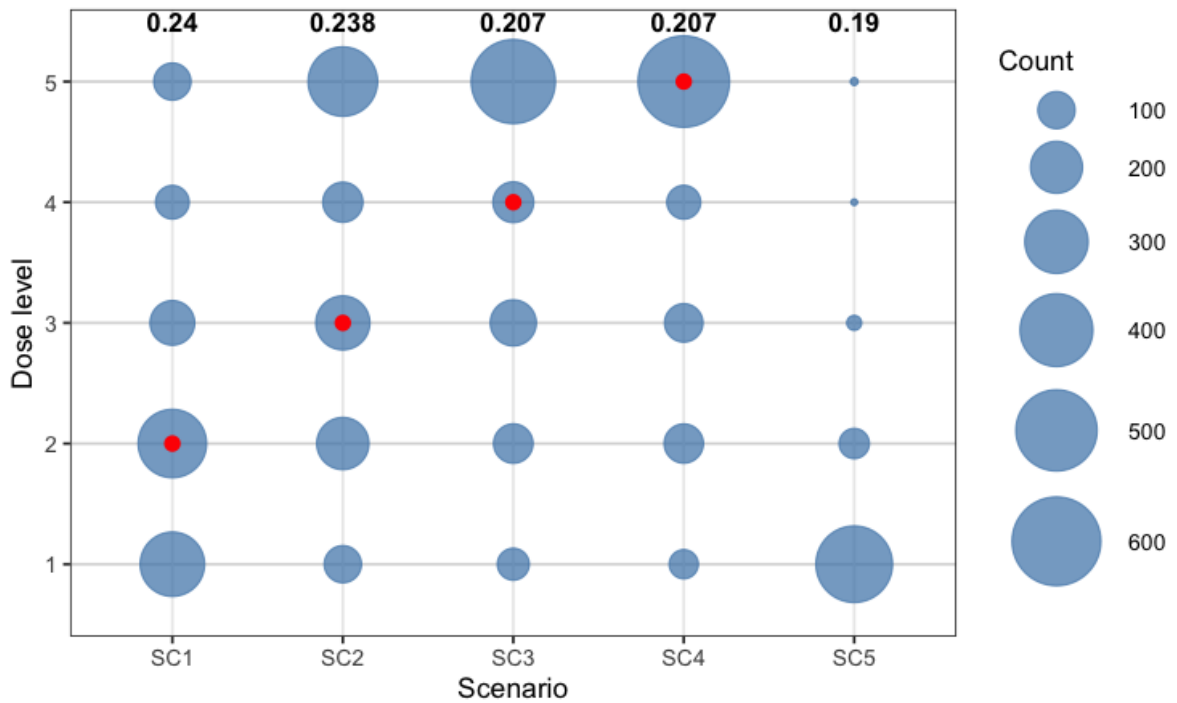


Figure 3.1: Dose assignment for the last patient treated in the precision dose-finding stage. Bubbles represent the number of times patient 30 in each simulated trial is assigned to each dose level in each scenario. The numbers above the bubble columns report the proportion of DLTs patient 30 experienced in 1,000 trials in each scenario. Red points denote the true MTD of the corresponding scenario.

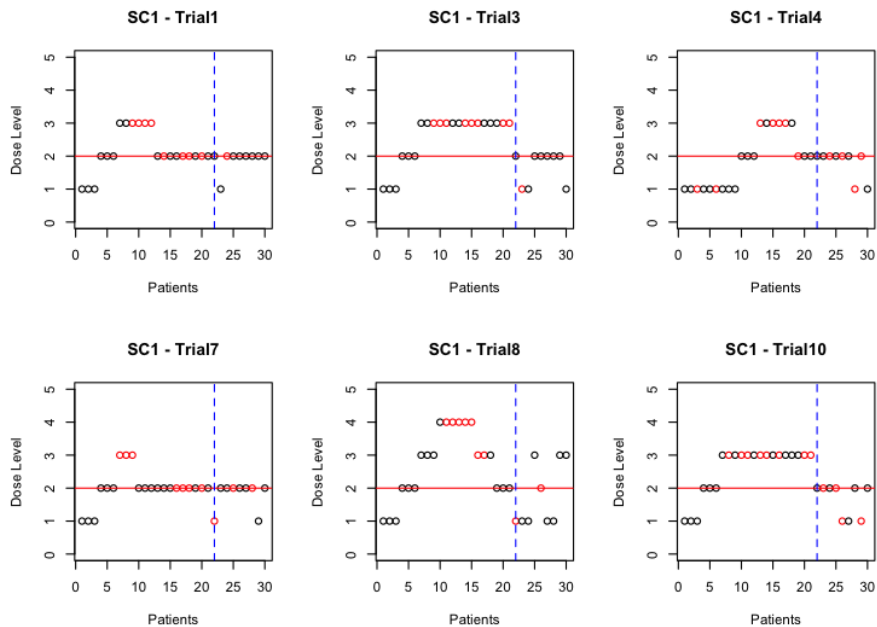


Figure 3.2: Dose assignments and DLT outcomes of six trials in scenario 1. Each point represents a patient. Black points: no DLT occurred; Red points: DLT occurred; Red horizontal lines: true MTD; Blue vertical dashed lines: start of precision dose-finding.

k_i increases, the predicted MTD also increases, implying a fast elimination rate helps increase tolerance to toxicity. Similarly, when V_i increases, the predicted MTD also increases. For example, given $k_i = 4$, the predicted MTD is dose level 3, 4, and 5 for V_i value of 2.95, 4.01, and 6.5, respectively. This is also sensible if the toxicity is inversely related to V_i as indicated in model (4).

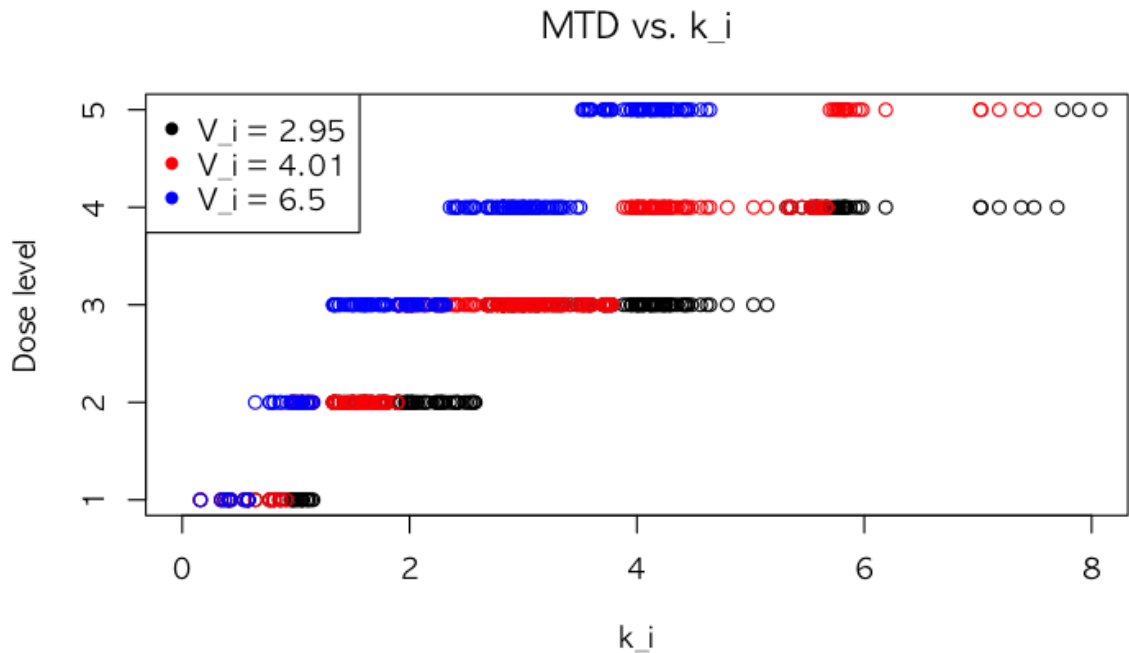


Figure 3.3: Examples of three volumes of distribution V_i with varying elimination rate constants k_i and their corresponding MTD. Each point represents a patient.

3.3 Sensitivity Analysis

3.3.1 PK Parameter Priors

As mentioned earlier, the choice of prior distributions for V_i and k_i is not restricted in our approach. Pharmacokinetic parameters such as clearance and volume of distribution are commonly modeled using log-normal distributions to ensure positivity and to capture the right-skewed nature of inter-individual variability (Mould and Upton, 2013). In particular, the SDF design assumes that both V_i and k_i follow log-normal distributions, while the PEDOOP design assumes gamma distributions for computational convenience. Motivated by this standard practice, we additionally conduct a sensitivity analysis in which

V_i and k_i are modeled using log-normal distributions instead of the gamma priors:

$$V_i \sim \log N(\mu_V, \sigma_V^2), k_i \sim \log N(\mu_k, \sigma_k^2).$$

We re-express the log-normal distribution parameters in terms of α and λ , while maintaining the same mean and variance as those used in the gamma distributions introduced in Section 3.1.

Table A.1 and Table A.2 (See Appendix) summarize the results of the sensitivity analysis compared to CRM. For the first 21 patients, our approach performs comparably to CRM in the first three scenarios, reasonably assigning patients and accurately identifying the MTD. However, in scenario 4, the PDF design selects a dose one level lower than the true MTD, while CRM successfully identifies it. In the final scenario, our approach results in a much lower Sel% at toxic doses.

Regarding the precision dose-finding phase, the PDF design remains relatively safe across the first four scenarios and dose levels. However, in scenario 5, the value of Y_d^*/n_d^* is generally higher. This can be attributed to the change in the assumptions about the PK model.

3.3.2 Stage I–Stage II Allocation Ratios

The experiments above were conducted under a Stage I–Stage II allocation ratio of 7:3, although the proposed design readily accommodates other allocation ratios. To assess robustness with respect to this design choice, we conducted a sensitivity analysis under alternative allocation ratios of 5:5 and 6:4 in scenario 1, and compared the results with those of CRM under sample sizes of 15 and 18. The results are summarized in Appendix Table A.4 and Table A.5. Across these settings, our method continues to outperform CRM in terms of operating characteristics, including assigning fewer patients to highly toxic doses and achieving higher accuracy in selecting the MTD, as well as selecting less toxic doses as the MTD. In addition, the observed toxicity rates, measured by Y_d^*/n_d^* , remain well controlled below the target level.

4 Discussion

In this paper, we extend the PEDOOP (Yuan et al., 2024) and the SDF designs (Su et al., 2022; Yang and Li, 2024) by proposing a Bayesian statistical model for the dose-toxicity relationship that simultaneously enables precision dose-finding. Our model inherits the strengths of the SDF designs, which leverage full PK profiles rather than relying on a summary PK measure, and incorporates the use of AUC as a covariate, as proposed in PEDOOP. However, unlike PEDOOP, which models toxicity probabilities at each dose level, our approach constructs a patient-specific model and uses posterior predictive probabilities to predict the toxicity risk for new patients in upcoming cohorts. Moreover, in contrast to PEDOOP, our model imposes no restrictions on the prior distributions of the volume of distribution and elimination rate constant, as long as they are clinically reasonable. A key innovation of our model is the new dose-finding framework, which assigns doses based on each patient’s individual toxicity probability. Simulation results demonstrate that our approach is valid and safe, with low risk of overdosing. One potential benefit of this framework is that it enables early-phase trials to generate insights into PK-toxicity relationships, which may be informative for later-phase trials.

A prerequisite for the PDF design is an accurate *pre-dose* prediction of each patient’s PK profile. A future direction is utilizing population pharmacokinetic (popPK) modeling for relating baseline covariates like body size, renal or hepatic function, and pharmacogenomic markers to key PK parameters. For example, by fitting a mixed-effects model to the first 21 participants’ rich PK samples, one can derive covariate effects and obtain patient-specific predictions for clearance CL_i and volume V_i , from which k_i can be computed via $k_i = CL_i/V_i$. Developing and validating such covariate-based popPK prediction models is beyond the scope of this paper. Instead, to reflect practical uncertainty in pre-dose PK prediction, we conducted simulations that introduce prediction errors into (V_i, k_i) and evaluate the robustness of Stage II dose assignment (Table 3.3). Such model-informed precision dosing has been advocated in oncology and therapeutic drug monitoring, and hybrid statistical/machine-learning approaches have re-

cently shown improved accuracy for antibiotics and targeted therapies (Iasonos and O’Quigley, 2014; Ma et al., 2024). Alternatively, step-up (or intra-patient titration) dosing can serve as a potential solution. Under this approach, each Stage II patient first receives a conservative priming dose, followed by sparse PK sampling. These early PK measurements can then be used, together with appropriate pharmacokinetic models, to predict patient-specific PK parameter for the full dose and make subsequent dosing decisions. Deploying these predictions prospectively for the remaining patients enables one-by-one dose assignments while maintaining the Bayesian coherence of the PDF design.

As in PEDOOP, we assume monotonicity of toxicity with respect to dose and use a first-order one-compartment model for IV injection. However, in practice, toxicity may not increase monotonically with dose and may instead follow a biphasic pattern, for example. Likewise, kinetic processes beyond first-order are possible. Thus, future work could explore extensions of our model that accommodate more flexible PK dynamics.

A potential limitation of our method is the computational burden, especially during the precision dose-finding process described in Section 2.4, where MCMC sampling is used to update model parameters after each patient’s enrollment. We report the running time of Stage I, Stage II, and the total procedure separately in Table A.3.

Although our method does not define a single population-level MTD by combining data from Stage I and Stage II, it is designed to identify an individualized MTD for each patient. Such patient-specific dose recommendations can be particularly valuable for patients who require urgent treatment, where individualized risk–benefit considerations are critical. Moreover, if dose assignments in Stage II exhibit substantial variability across patients, clinicians may reasonably hesitate to recommend a single MTD for the entire population based solely on Stage I results, as this variability suggests meaningful heterogeneity in dose tolerance. In addition, as noted in PEDOOP, modern phase I trials are increasingly encouraged to identify the optimal biological dose (OBD), which motivates incorporating efficacy outcomes alongside toxicity. Given that toxicities may emerge late in treatment, identifying doses based solely on a toxicity

endpoint may be inadequate (Tosi et al., 2015). Therefore, future enhancements to the PDF design could be made from this perspective.

In Section 2.4, we set the Stage I size to 70% of the total number of patients, following a commonly used sample size in phase I trials. The sensitivity analysis indicates that our approach is robust to the choice of Stage I–Stage II allocation ratios. Nevertheless, we recommend setting the Stage I sample size larger than the number of dose levels, so that all investigational doses can be adequately explored before proceeding to Stage II. In addition, computational considerations may arise when the Stage II sample size becomes larger, since posterior updates are performed sequentially as each patient is enrolled. As an extension, we aim to explore the sample size determined by an iterative criterion – e.g., measuring convergence in posterior summaries of model parameters – to assess whether the trial is ready to enter the precision dose-finding stage. Alternatively, one could estimate the minimum training sample size required to support reliable inference. Otherwise, we recommend finding the desirable allocation ratio based on simulations using the PDF design.

References

Babb, J. S. and Rogatko, A. (2001). Patient specific dosing in a cancer phase i clinical trial. *Statistics in Medicine*, 20(14):2079–2090.

Cheung, Y. K. (2005). Coherence principles in dose-finding studies. *Biometrika*, 92(4):863–873.

Goodman, S. N., Zahurak, M. L., and Piantadosi, S. (1995). Some practical improvements in the continual reassessment method for phase I studies. *Statistics in Medicine*, 14(11):1149–1161.

Guo, W., Wang, S.-J., Yang, S., Lynn, H., and Ji, Y. (2017). A Bayesian interval dose-finding design addressing Ockham’s razor: mTPI-2. *Contemporary Clinical Trials*, 58:23–33.

Iasonos, A. and O’Quigley, J. (2014). Adaptive dose-finding studies: a review of model-guided phase i clinical trials. *Journal of Clinical Oncology*, 32(23):2505–2511.

Ji, Y., Li, Y., and Bekele, B. N. (2007). Dose-finding in phase I clinical trials based on toxicity probability intervals. *Clinical Trials*, 4(3):235–244. PMID: 17715248.

Ji, Y., Liu, P., Li, Y., and Bekele, B. N. (2010). A modified toxicity probability interval method for dose-finding trials. *Clinical Trials*, 7(6):653–663. PMID: 20935021.

Liu, M., Wang, S.-J., and Ji, Y. (2020). The i3+3 design for phase I clinical trials. *Journal of Biopharmaceutical Statistics*, 30(2):294–304. PMID: 31304864.

Liu, S. and Yuan, Y. (2015). Bayesian optimal interval designs for phase I clinical trials. *Journal of the Royal Statistical Society. Series C: Applied Statistics*, 64(3):507–523.

Ma, P., Ma, H., Liu, R., Wen, H., Li, H., Huang, Y., Li, Y., Xiong, L., Xie, L., and Wang, Q. (2024). Prediction of vancomycin plasma concentration in elderly patients based on multi-algorithm mining combined with population pharmacokinetics. *Scientific Reports*, 14:27165.

Mould, D. and Upton, R. (2013). Basic concepts in population modeling, simulation, and model-based drug development—part 2: Introduction to pharmacokinetic modeling methods. *CPT: Pharmacometrics & Systems Pharmacology*, 2(4):38.

Nikanjam, M., Kato, S., Sicklick, J. K., and Kurzrock, R. (2023). At the right dose: personalised (n-of-1) dosing for precision oncology. *European Journal of Cancer*, 194:113359.

Ollier, A. and Mozgunov, P. (2025). On inclusion of covariates in model based dose finding clinical trial designs. *Statistics in Medicine*, 44(3–4):e10337.

O’Quigley, J., Pepe, M., and Fisher, L. (1990). Continual reassessment method: A practical design for phase 1 clinical trials in cancer. *Biometrics*, 46(1):33–48.

Piantadosi, S. and Liu, G. (1996). Improved designs for dose escalation studies using pharmacokinetic measurements. *Statistics in Medicine*, 15(15):1605–1618.

Robertson, T., Wright, F., and Dykstra, R. (1988). *Order Restricted Statistical Inference*. Probability and Statistics Series. Wiley.

Shargel, L., Andrew, B., and Wu-Pong, S. (1999). *Applied biopharmaceutics & pharmacokinetics*, volume 264. Appleton & Lange Stamford, Stamford, Connecticut, USA.

Silva, R. B., Cheng, B., Carvajal, R. D., and Lee, S. M. (2024). Dose individualization for phase i cancer trials with broadened eligibility. *Statistics in Medicine*, 43(29):5534–5547. Epub 2024 Oct 31.

Storer, B. E. (1989). Design and analysis of phase I clinical trials. *Biometrics*, 45(3):925–937.

Su, X., Li, Y., Müller, P., Hsu, C.-W., Pan, H., and Do, K.-A. (2022). A semi-mechanistic dose-finding design in oncology using pharmacokinetic pharmacodynamic modeling. *Pharmaceutical Statistics*, 21(6):1149–1166.

Tosi, D., Laghzali, Y., Vinches, M., Alexandre, M., Homicsko, K., Fasolo, A., Del Conte, G., Durigova, A., Hayaoui, N., Gourgou, S., Gianni, L., and Mollevi, C. (2015). Clinical development strategies and outcomes in first-in-human trials of monoclonal antibodies. *Journal of Clinical Oncology*, 33(19):2158–2165. PMID: 26014300.

Toumazi, A., Comets, E., Alberti, C., Friede, T., Lentz, F., Stallard, N., Zohar, S., and Ursino, M. (2018). dfpk: An r-package for bayesian dose-finding designs using pharmacokinetics (pk) for phase i clinical trials. *Computer Methods and Programs in Biomedicine*, 157:163–177.

Ursino, M., Zohar, S., Lentz, F., Alberti, C., Friede, T., Stallard, N., and Comets, E. (2017). Dose-finding methods for phase I clinical trials using pharmacokinetics in small populations. *Biometrical Journal*, 59(4):804–825.

Whitehead, J., Zhou, Y., Hampson, L., Ledent, E., and Pereira, A. (2007). A Bayesian approach for dose-escalation in a phase I clinical trial incorporating pharmacodynamic endpoints. *Journal of Biopharmaceutical Statistics*, 17(6):1117–1129. PMID: 18027220.

Yang, C. and Li, Y. (2024). An extended bayesian semi-mechanistic dose-finding design for phase i oncology trials using pharmacokinetic and pharmacodynamic information. *Statistics in Medicine*, 43(4):689–705.

Yuan, S., Huang, Z., Liu, J., and Ji, Y. (2024). Pharmacometrics-Enabled DOse OPtimization (PEDOOP) for seamless phase I-II trials in oncology. *Journal of Biopharmaceutical Statistics*, 0(0):1–20. PMID: 38888933.

Appendix

A.1 Sensitivity Analysis Results

Table A.1: Simulation results of the first 21 patients of scenarios 1 to 5 under log-normal distributions.

		Dose levels	1	2	3	4	5	No MTD
SC 1	PDF	True avg p_d	0.128	0.263	0.455	0.578	0.661	–
		Y_d/n_d	0.139	0.269	0.434	0.607	0.544	–
		n_d	5.982	8.493	5.439	0.960	0.057	–
	CRM	Sel%	0.129	0.480	0.337	0.044	0.005	0.005
		n_d	6.585	7.863	5.451	1.035	0.066	–
	CRM	Sel%	0.098	0.475	0.369	0.054	0.004	0.000
SC 2	PDF	True avg p_d	0.056	0.132	0.269	0.378	0.463	–
		Y_d/n_d	0.066	0.134	0.283	0.377	0.433	–
		n_d	3.846	5.274	7.074	3.909	0.897	–
	CRM	Sel%	0.010	0.141	0.410	0.331	0.108	0.000
		n_d	3.843	5.214	6.960	3.969	1.014	–
	CRM	Sel%	0.001	0.095	0.356	0.400	0.148	0.000
SC 3	PDF	True avg p_d	0.036	0.089	0.195	0.287	0.365	–
		Y_d/n_d	0.039	0.092	0.210	0.288	0.354	–
		n_d	3.450	4.326	6.111	4.932	2.181	–
	CRM	Sel%	0.003	0.048	0.248	0.417	0.284	0.000
		n_d	3.468	4.176	6.075	4.836	2.445	–
	CRM	Sel%	0.000	0.018	0.193	0.392	0.397	0.000
SC 4	PDF	True avg p_d	0.104	0.149	0.208	0.250	0.282	–
		Y_d/n_d	0.118	0.147	0.217	0.254	0.287	–
		n_d	4.818	5.097	5.631	3.630	1.773	–
	CRM	Sel%	0.025	0.087	0.283	0.327	0.275	0.003
		n_d	4.725	5.229	5.667	3.471	1.908	–
	CRM	Sel%	0.007	0.100	0.237	0.324	0.332	0.000
SC 5	PDF	True avg p_d	0.406	0.584	0.744	0.818	0.861	–
		Y_d/n_d	0.414	0.592	0.710	0.444	0	–
		n_d	13.080	2.796	0.210	0.009	0	–
	CRM	Sel%	0.508	0.051	0.004	0.001	0	0.436
		n_d	18.906	1.917	0.177	0	0	–
	CRM	Sel%	0.944	0.055	0.001	0	0	0.000

Table A.2: Simulation results of the last nine patients of scenarios 1 to 5 under log-normal distributions.

Dose levels		1	2	3	4	5
SC 1	True avg p_d	0.128	0.263	0.455	0.578	0.661
	Y_d^*/n_d^*	0.320	0.220	0.276	0.332	0.208
	n_d^*	2.359	3.055	1.647	0.651	1.203
SC 2	True avg p_d	0.056	0.132	0.269	0.378	0.463
	Y_d^*/n_d^*	0.326	0.232	0.239	0.250	0.170
	n_d^*	0.680	1.639	1.904	1.367	3.397
SC 3	True avg p_d	0.036	0.089	0.195	0.287	0.365
	Y_d^*/n_d^*	0.337	0.252	0.254	0.235	0.150
	n_d^*	0.371	0.927	1.322	1.309	5.067
SC 4	True avg p_d	0.104	0.149	0.208	0.250	0.282
	Y_d^*/n_d^*	0.287	0.292	0.290	0.238	0.160
	n_d^*	0.537	0.888	1.137	1.120	5.289
SC 5	True avg p_d	0.406	0.584	0.744	0.818	0.861
	Y_d^*/n_d^*	0.358	0.301	0.338	0.433	0.200
	n_d^*	3.780	0.655	0.142	0.030	0.035

Table A.3: Computation time (seconds) for Stage I, Stage II, and total runtime of a single simulated trial.

Scenario	Stage I (s)	Stage II (s)	Total (s)
SC 1	15.393	21.670	37.064
SC 2	15.115	23.295	38.410
SC 3	15.592	21.878	37.470
SC 4	15.217	22.014	37.230
SC 5	7.178	0.000	7.178

Table A.4: Stage I simulation results for scenario 1 under varying Stage I–Stage II allocation ratios

		Dose levels	1	2	3	4	5
Stage I: 50% Stage II: 50%	True avg p_d	0.151	0.287	0.470	0.586	0.665	
	PDF	Y_d/n_d	0.151	0.287	0.478	0.609	0.333
		n_d	5.589	6.156	2.847	0.297	0.003
		Sel%	0.164	0.517	0.284	0.024	0.001
	CRM	n_d	6.396	5.460	2.775	0.363	0.006
		Sel%	0.204	0.412	0.279	0.089	0.016
Stage I: 60% Stage II: 40%	True avg p_d	0.151	0.287	0.470	0.586	0.665	
	PDF	Y_d/n_d	0.150	0.290	0.479	0.608	0.417
		n_d	5.922	7.476	3.942	0.510	0.012
		Sel%	0.156	0.551	0.247	0.034	0.002
	CRM	n_d	7.224	6.618	3.549	0.588	0.021
		Sel%	0.190	0.458	0.302	0.045	0.005

Table A.5: Stage II simulation results for scenario 1 under varying Stage I–Stage II allocation ratios

		Dose levels	1	2	3	4	5
Stage I: 50% Stage II: 50%	True avg p_d	0.151	0.287	0.470	0.586	0.665	
		Y_d^*/n_d^*	0.342	0.203	0.262	0.233	0.209
		n_d^*	4.225	4.567	2.269	1.202	2.513
	True avg p_d	0.151	0.287	0.470	0.586	0.665	
		Y_d^*/n_d^*	0.329	0.192	0.257	0.274	0.197
		n_d^*	3.511	4.069	1.937	0.764	1.557
Stage I: 60% Stage II: 40%	True avg p_d	0.151	0.287	0.470	0.586	0.665	
		Y_d^*/n_d^*	0.329	0.192	0.257	0.274	0.197
		n_d^*	3.511	4.069	1.937	0.764	1.557
	True avg p_d	0.151	0.287	0.470	0.586	0.665	
		Y_d^*/n_d^*	0.329	0.192	0.257	0.274	0.197
		n_d^*	3.511	4.069	1.937	0.764	1.557